Research Square

Preprints are preliminary reports that have not undergone peer review.
They should not be considered conclusive, used to inform clinical practice,
or referenced by the media as validated information.

PIP4K2A-derived peptide PIP4-1 exhibits preferential antitumor activity in PTEN- deficient and patient-derived glioblastoma models

Yong-Jun Kwon
Luxembourg Institute of Health
Yunjeong Oh
Samsung Medical Center
Jinhee Kim
Samsung Medical Center
Yong Jae Shin
yongjae.shin@samsung.com

Samsung Medical Center

Article

Keywords: glioblastoma, PIP4K2A, PTEN, cell-penetrating peptide, temozolomide, patient-derived model

Posted Date: November 3rd, 2026

DOI: https://doi.org/10.21203/rs.3.rs-11200524/v1

License: This work is licensed under a Creative Commons Attribution 4.0 International License.
Read Full License

Additional Declarations: No competing interests reported.

Abstract

Glioblastoma (GBM) remains incurable despite surgery, radiotherapy and temozolomide (TMZ) chemotherapy, and molecular heterogeneity, therapy resistance and limited intracranial drug exposure sustain the need for pharmacologically distinct agents that are active in patient-relevant models. Because PIP4K2A restrains tumour progression in PTEN-deficient glioblastoma, we screened twelve cell-penetrating peptides derived from PIP4K2A in PDC1, a patient-derived culture in which PTEN and PIP4K2A protein were undetectable. PIP4-1 demonstrated the most reproducible concentration-dependent activity across two- and three-dimensional PDC1 cultures and retained activity in PDC4. In an exploratory murine comparison, PIP4-1 reduced viability to approximately 15% of control in PTEN-deficient GL26 cells but only to approximately 85% in PTEN-expressing GL261 cells ($P = 4.69 \times 10^{-5}$), identifying PTEN-low status as a candidate response context. At 200 µg/mL, PIP4-1 reduced viability more than 500 µM temozolomide in PDC1 and PDC4, although these models are not annotated for TMZ resistance. In a pilot subcutaneous xenograft study, PIP4-1 significantly reduced terminal tumour volume relative to vehicle. Keratinocyte and liver-organoid assays provided an initial tolerability context, suggesting a favorable safety profile. These data prioritize PIP4-1 as a lead candidate requiring mechanistic validation, selectivity assessment, stability and exposure studies, and efficacy testing in annotated orthotopic models.

Introduction

Glioblastoma is the most aggressive adult diffuse glioma. Contemporary classification restricts this diagnosis to IDH-wildtype tumors [1], while recurrence is nearly universal and survival remains poor despite multimodal treatment [2, 3], which continues to comprise maximal safe resection followed by radiotherapy and temozolomide[4, 5]. Therapeutic development is further constrained by inter- and intratumoral heterogeneity, dynamic cellular states, and limited drug delivery across the blood-brain and blood-tumor barriers [6–10].

Alterations affecting the PTEN–PI3K–AKT axis are common in glioblastoma and remain biologically important, although PTEN status is not yet an established treatment-selection biomarker in adult glioma [8–11]. PTEN normally restrains PI3K signaling, whereas PTEN loss can promote proliferative and survival programs associated with aggressive disease and treatment resistance [12–17]. Therapeutically restoring tumor-suppressor function is challenging because PTEN itself is not a conventional druggable target.

PIP4K2A is a phosphoinositide kinase reported to restrain tumor progression in PTEN-deficient glioblastoma, in part through attenuation of PI3K signaling [18]. We therefore asked whether short PIP4K2A-derived sequences coupled to a cell-penetrating carrier could serve as a starting point for peptide therapy. Advances in peptide therapeutics and cell-penetrating carriers support this strategy, but pharmacological development requires evidence of sequence-dependent activity, cancer-cell selectivity, stability, cellular uptake, exposure, and tolerability [19–24]. Throughout this report, “PIP4K2A-derived”

denotes sequence origin only and does not imply that a peptide reproduces the catalytic or signaling function of full-length PIP4K2A.

Patient-derived glioblastoma cultures and three-dimensional models can retain clinically relevant tumor phenotypes and heterogeneity, supporting their use in preclinical screening and functional assessment [25–30]. Patient-derived xenografts provide a complementary system for initial in vivo evaluation [31–33]. We therefore mapped and screened a panel of PIP4K2A-derived peptides in patient-derived glioblastoma cells and spheroids, and then prioritized active candidates through concentration-response testing, a PTEN-differential comparison, benchmarking against temozolomide, a pilot xenograft experiment, and preliminary assessment in nonmalignant models. The study was designed to identify a reproducibly active lead and to generate testable biomarker and development hypotheses, not to establish a complete mechanism of action.

Results

Patient-derived screening identifies PIP4-1 as a lead peptide

Twelve peptide sequences were selected from different regions of human PIP4K2A, including conserved and nonconserved regions within the PIPK domain (residues 33–405; Fig. 1A). The candidate sequences ranged from 11 to 25 amino acids and were joined through a glycine–glycine spacer to the polybasic cell-penetrating carrier CKSKRRRRRRSKRKD. The panel was designed to sample spatially distinct regions of PIP4K2A rather than to reproduce the catalytic function of the full-length protein.

Selected peptide regions were mapped onto the PIP4K2A crystal structure (PDB 2YBX; Fig. 1B). PIP8 (residues 54–66), PIP12 (67–91), PIP2 (91–106), and PIP4 (182–192) occupied distinct structural regions; the model also displays a highlighted segment at residues 73–83. This mapping illustrates the spatial origin of the candidate sequences but does not establish cellular accessibility, molecular interaction, catalytic activity, or functional mimicry of full-length PIP4K2A.

PDC1 was selected as the initial screening model because PTEN and PIP4K2A proteins were undetectable under the immunoblot conditions used in this study (Fig. 2A). Previous work showing that PIP4K2A restrains PI3K signaling and tumor progression in PTEN-deficient glioblastoma provided the biological rationale for screening PIP4K2A-derived peptides in this molecular context [18]; PDC1 was therefore used as a potentially sensitized system for lead identification. However, this model-selection rationale does not definitively demonstrate that peptide activity depends on the absence of PTEN or PIP4K2A.

The 12 constructs were screened in PDC1 using dissociated 2D cultures and 3D spheroids. In 2D cultures, most peptides had limited effects at lower concentrations, whereas several constructs reduced viability at the upper end of the tested range (Fig. 1C). PIP4-1 showed one of the clearest concentration-related responses in this format, whereas PIP2-1, PIP5-1, PIP6-1, PIP8-1, and PIP12-1 produced smaller reductions. The response profile differed partially in 3D spheroids (Fig. 1D): PIP12-1 produced the largest

reduction at the highest tested concentration, while PIP4-1, PIP5-1, PIP8-1, and PIP9-1 also showed measurable activity. No construct was therefore uniformly dominant across conditions. PIP4-1 was prioritized because it produced a reproducible concentration-related response in both culture formats, rather than because it produced the largest effect in any single assay.

Lead activity across patient-derived and PTEN-differential glioma models

The immunoblot showed heterogeneous PTEN and PIP4K2A expression across NHA and PDC1–PDC7 (Fig. 2A). Both proteins were undetectable in PDC1 and PDC4 under the evaluated conditions, while other models retained one or both proteins. In the PDC4 fixed-dose experiment, the magnitude of viability reduction differed among PIP4-1, PIP8-1, PIP12-1, and PIP4/12 − 1 and was generally greater at 200 than at 100 µg/mL (Fig. 2B). PIP4-1, PIP8-1, and PIP4/12 − 1 each produced significant, dose-dependent reductions in viability, whereas PIP12-1 did not reach significance at either dose; temozolomide produced a small but statistically significant reduction only at 500 µM (full statistics in the Fig. 2 legend). MTT experiments in PDC1 showed distinct concentration-response profiles for PIP12-1, PIP4-2, and PIP11-2 (Supplementary Figure S1). Modified PIP4-1 constructs also produced model-dependent effects in PDC4, with strong activity for selected cyclized or palmitoylated variants but no uniform improvement across constructs, and construct effects differed significantly by one-way ANOVA at both tested concentrations (Supplementary Figure S2). Their architectures and sequences are summarized in Supplementary Figure S3 and Supplementary Table S1.

In the exploratory murine comparison, PIP4-1 reduced viability to approximately 15% of control in PTEN-deficient GL26 cells, compared with approximately 85% in PTEN-expressing GL261 cells (Fig. 2C), a difference that remained significant after correction for multiple comparisons ($P = 4.69 \times 10^{-5}$). This was the largest PTEN-associated response difference among the tested peptides and identifies PTEN-low or PTEN-null status as a candidate sensitivity context for PIP4-1. PIP8-1 showed a smaller difference that did not survive correction, whereas PIP12-1 and PIP4/12 − 1 produced similar responses in the two lines. Temozolomide showed a nominal but non-significant difference between GL26 and GL261 ($P = 0.194$), indicating that, unlike PIP4-1, its activity did not track PTEN status in this comparison.

Fixed-dose peptide and temozolomide responses in patient-derived cultures

Figure 3 compares PIP4-1, PIP8-1, PIP12-1, and PIP4/12 − 1 at 40 and 200 µg/mL, with or without 500 µM temozolomide, in PDC1 and PDC4. PIP4-1 at 200 µg/mL produced a pronounced viability reduction in both models and was more active than temozolomide alone under the assay conditions shown: temozolomide reduced viability only partially, to approximately 50–60% of control, whereas 200 µg/mL PIP4-1 reduced viability to markedly lower levels. At 40 µg/mL, adding PIP4-1 to temozolomide produced a further reduction in viability relative to PIP4-1 alone in both PDC1 and PDC4. In both models, every peptide dose, temozolomide, and combination condition significantly reduced viability relative to control, and adding temozolomide to peptide at 40 µg/mL produced a significantly greater reduction than peptide alone for every peptide (full statistics in the Fig. 3 legend). These observations support further

evaluation of PIP4-1 in glioblastoma models with limited temozolomide responsiveness, but they are assay-specific activity comparisons and not evidence of superior potency.

Antitumor activity in a subcutaneous xenograft model

To determine whether the differential peptide activity observed in vitro was retained in vivo, PIP4-1, PIP8-1, and PIP4/12 − 1 were evaluated at 100 mg/kg in mice bearing subcutaneous PDX4 xenografts (n = 3 per group; Fig. 4). Consistent with the cell-based findings, the PIP4-1 and PIP8-1 groups followed lower mean tumor-volume trajectories than the vehicle group, whereas PIP4/12 − 1 showed limited and less consistent activity. Terminal tumor volumes differed significantly among groups, with a significant reduction for PIP4-1 versus vehicle but not for PIP8-1 or PIP4/12 − 1 (full statistics in the Fig. 4 legend). This pilot experiment therefore reproduced the relative response pattern observed in vitro and provides initial in vivo support for PIP4-1 as an active lead, with a consistent but statistically unconfirmed trend for PIP8-1. Body weight over the dosing period is shown in Supplementary Figure S4.

Preliminary tolerability in nonmalignant models

HaCaT viability remained near control levels at 200 and 400 μg/mL PIP4-1 but fell markedly at 800 μg/mL (Fig. 5A). In normal liver organoids, PIP4-1 and PIP12-1 largely preserved viability through 200 μg/mL, whereas PIP8-1 reduced viability at the highest concentration (Figs. 5B–D). A separate fixed-dose experiment showed modest, construct-dependent organoid effects at 200 μg/mL, with PIP4/12 − 1 producing the largest reduction among the displayed peptides (Fig. 5E). Albumin measurements at days 4 and 7 remained broadly within the control range across most conditions (Fig. 5G). These cross-model data provide an initial concentration-based tolerability context; because the malignant and nonmalignant assays were not matched for assay platform, exposure duration, or tissue origin, a quantitative cancer-cell selectivity index was not calculated.

Discussion

This study used complementary screening formats to systematically prioritize PIP4-1 pharmacologically from 12 PIP4K2A-derived cell-penetrating peptides. PIP4-1 combined a reproducible concentration-related response in dissociated PDC1 cells and three-dimensional spheroids, activity in PDC4, a marked response in PTEN-deficient GL26 cells, activity exceeding temozolomide under the fixed-dose conditions shown, and retention of the relative lead pattern in a pilot xenograft experiment. The two- and three-dimensional rankings were not identical, which is expected when tissue architecture alters penetration, cellular state, stability, and effective exposure. Cross-format reproducibility, rather than maximal activity in a single condition, therefore provided the principal basis for lead selection.

The absence of detectable PTEN and PIP4K2A proteins provided a biologically relevant context for using PDC1 as the initial screening model, because PIP4K2A has been shown to restrain PI3K signaling and tumor progression in PTEN-deficient glioblastoma[18] [18]. A PTEN/PIP4K2A-undetectable model therefore offered a rational setting in which to search for active PIP4K2A-derived sequences. Screening

in a single molecularly selected model may nevertheless favour compounds that are active in that particular cellular background, and the present experiments do not demonstrate that PIP4-1 restores PIP4K2A function or that its activity requires PTEN or PIP4K2A deficiency.

The GL26/GL261 comparison supports PTEN status as a biomarker hypothesis rather than a demonstrated determinant of response. PIP4-1 produced the largest differential among the tested peptides, with deep viability reduction in PTEN-deficient GL26 and limited activity in PTEN-expressing GL261. This pattern is biologically compatible with the reported relationship between PIP4K2A and PI3K signaling in PTEN-deficient glioblastoma. However, GL26 and GL261 are biologically distinct lines rather than an isogenic pair, and temozolomide did not differ significantly between them ($P = 0.194$), so background differences beyond PTEN status cannot be excluded. Direct PTEN knockout and rescue in matched backgrounds, together with PIP4K2A perturbation, carrier-only and sequence-randomized controls, and early pathway readouts such as AKT and mTOR phosphorylation, will be required to determine whether PTEN loss causally sensitizes cells to PIP4-1.

The fixed-dose experiments generate a second development hypothesis. At 200 µg/mL, PIP4-1 reduced viability more strongly than 500 µM temozolomide in PDC1 and PDC4. This result is relevant to tumors in which temozolomide activity is limited, but it should be read as an assay-specific activity comparison rather than as evidence of superior potency or of clinical dosing feasibility; the two agents differ in molar concentration, mechanism, and exposure kinetics. Temozolomide retained partial activity, and MGMT promoter methylation, MGMT expression, prior drug exposure, and clinical resistance history were unavailable for these models. PIP4-1 should therefore be tested across full concentration-response curves in molecularly annotated, experimentally induced, and clinically derived temozolomide-resistant models.

The PDX4 xenograft pilot reproduced the relative in vitro candidate pattern: PIP4-1 and PIP8-1 were associated with lower tumor-volume trajectories than vehicle, whereas PIP4/12 – 1 showed limited and less consistent activity. This concordance supports progression of the active leads, but it does not substitute for an adequately powered efficacy study; with three animals per group the experiment can detect only large effects and provides no reliable estimate of effect size. Dose exposure, route-dependent bioavailability, plasma and tissue stability, intracranial distribution, pharmacokinetics, and pharmacodynamic target engagement remain unknown. These parameters are particularly important for a polybasic cell-penetrating peptide intended for brain-tumor development, because subcutaneous xenografts do not model the blood–brain and blood–tumor barriers.

Limitations and next development steps

The study was intentionally designed for lead identification and therefore establishes reproducible activity patterns rather than complete pharmacological characterization. Its principal advances are the consistent prioritization of PIP4-1 across patient-derived two- and three-dimensional models, a strong PTEN-associated response difference that can be tested experimentally, activity in models with limited

temozolomide response, and in vitro–in vivo concordance among selected peptides. The main limitations are the small in vivo cohort, the absence of matched malignant and nonmalignant assay conditions, the incomplete set of sequence-randomized and carrier-only controls in the primary screen, the lack of direct evidence for cellular uptake and target engagement, and the descriptive nature of the structural mapping. The immediate priorities are replicate-level statistical confirmation; matched malignant and nonmalignant testing; complete randomized-sequence and carrier-only controls; PTEN and PIP4K2A perturbation; uptake, stability, pharmacokinetic and pharmacodynamic studies; and powered orthotopic efficacy and safety experiments.

Overall, the data identify PIP4-1 as a pharmacologically prioritized preclinical lead and define two testable development contexts: PTEN-low glioblastoma and tumors with limited temozolomide responsiveness. Completing the package outlined above would distinguish a reproducibly cytotoxic screening lead from a mechanism-based therapeutic candidate.

Methods

Peptide design, synthesis, and characterization

Design and nomenclature of CPP-conjugated peptides. Twelve PIP4K2A-derived candidate sequences were coupled to a polybasic cell-penetrating peptide (CPP) carrier via a diglycine (–GG–) linker in an N-to-C orientation (PIP–GG–CPP) (Fig. 1A; Supplementary Table S1). PIP4-1 comprises PIP4K2A residues 182–192 (YRLNVDGVEIY) linked to the CPP sequence CKSKRRRRRRSKRKD. The nomenclature suffixes “-1” and “-2” designate C-terminal conjugation with the RMAD1 and RMMR1 carriers, respectively. Initial concentration-response screening included the constructs PIP12-1, PIP4-2, and PIP11-2, as well as the hybrid construct PIP4/12 – 1 (Supplementary Figure S1). On the basis of functional screening rather than structural modeling, PIP4-1 and PIP8-1 showed the greatest antitumor activity and were selected as lead scaffolds for sequence diversification and chemical optimization, which included cyclized, N-palmitoylated, and truncated variants alongside randomized-sequence and carrier-only negative controls (Supplementary Figures S2 and S3; Supplementary Table S1).

Peptide synthesis, N-palmitoylation, and purification. All linear and modified peptides were synthesized by standard Fmoc solid-phase peptide synthesis (Fmoc-SPPS) on Fmoc-Rink amide resin to yield C-terminally amidated products (–CONH2). Fmoc deprotection was performed with 20% piperidine in DMF, and amino acid couplings were mediated by TBTU and DIEA in DMF at room temperature, monitored by colorimetric testing. After peptide assembly, the N-terminal Fmoc group was removed and palmitic acid was coupled to generate N-palmitoylated derivatives. Peptidyl resins were cleaved with a standard TFA-based cocktail, and crude peptides were precipitated with cold diethyl ether. All final products were purified to > 95% purity by reverse-phase high-performance liquid chromatography (RP-HPLC) and verified by liquid chromatography–mass spectrometry (LC–MS); lot numbers, observed molecular weights, purity values, and formulation details are given in Supplementary Table S1.

Structural mapping

Candidate regions were displayed on the PIP4K2A crystal structure (PDB 2YBX, residues 35–405; Fig. 1B). The model identifies the sequence locations of PIP2, PIP4, PIP8, and PIP12 and an additional highlighted region at residues 73–83. Structural mapping was descriptive and did not test molecular binding, catalytic mimicry, or mechanism of action.

Patient-derived glioblastoma models

Patient-derived glioblastoma cultures are designated PDC1–PDC7. PDC1 was used for the initial dissociated-cell and spheroid screen and for the MTT concentration-response curves shown in Supplementary Figure S1. PDC4 was used for fixed-dose peptide testing, optimization experiments, peptide–temozolomide combinations, and the PDX4 xenograft pilot. PDC7 was used as a fixed-dose response model and was also included in the Fig. 2A immunoblot, in which PIP4K2A was weakly detected and PTEN was not detected. PTEN and PIP4K2A expression was evaluated in normal human astrocytes and PDC1–PDC7 (Fig. 2A; Supplementary Table S2). Patient-derived glioblastoma cultures (PDC1–PDC7) were established at Samsung Medical Center from surgical specimens obtained under Institutional Review Board approval No. 2010-04-004, with written informed consent from all donors.

Cell lines, provenance, and culture conditions

The murine glioma lines GL26 and GL261 were kind gifts from Dr. John S. Yu (Cedars-Sinai Medical Center, Los Angeles, CA, USA) and were maintained in RPMI-1640 supplemented with 10% fetal bovine serum. HaCaT keratinocytes were purchased from Koma Biotech Inc. (Seoul, Republic of Korea; Cat. No. BR1004, Human HaCaT Keratinocyte Starter Kit) and were cultured according to the supplier's instructions. All cell lines and patient-derived cultures were maintained at low passage number and were used within 20 passages of receipt or establishment. All lines were confirmed to be free of mycoplasma contamination by PCR using the BioMycoX® Mycoplasma PCR Detection Kit (Cat. No. D-100; Cellsafe, Republic of Korea). Cell lines were used as received from the supplier and from the donating laboratory, and were not independently re-authenticated by short tandem repeat profiling.

Cell culture, peptide treatment, and viability

Patient-derived primary glioblastoma cells (including PDC4) and neural progenitor cells (NPCs) were cultured in Neurobasal medium supplemented with N2, B27 (0.5× each; Invitrogen), and bFGF/EGF (25 ng/mL each; R&D Systems) as previously described [18].

For viability assays, cells were seeded in 384-well plates (500 cells/well) and incubated for 24 hours prior to treatment. Cells were treated for 72 hours with serial dilutions or fixed concentrations of candidate peptides (100 and 200 μg/mL for single agents, Fig. 2B; 40 or 200 μg/mL for combinations, Fig. 3) with or without temozolomide (100 or 500 μM). Vehicle controls received equal volumes of sterile PBS or DMSO (< 0.1% v/v).

Viability was determined using either an ATP-dependent luminescent assay or an MTT assay:

- **ATP luminescence**

viability was evaluated with the ATPlite 1step Luminescence Assay System according to the manufacturer's protocol and measured on an EnVision Multilabel Plate Reader (Revvity) or an Operetta CLS high-content screening system (PerkinElmer).

- **MTT assay**

cells were incubated with 0.5 mg/mL MTT (Sigma-Aldrich) for 4 h at 37°C, followed by formazan solubilization in DMSO; absorbance was recorded at 570 nm (reference 650 nm) on an xMark Microplate Spectrophotometer (Bio-Rad).

All assays were conducted with at least three technical replicates across three or more independent biological experiments ($n \geq 3$). Data were normalized to vehicle controls after background subtraction. Plates were qualified for analysis only when vehicle controls exhibited a coefficient of variation (CV) < 10%; wells with visible edge effects, air bubbles, or statistical outliers (Grubbs' test, $\alpha = 0.05$) were excluded prior to normalization. Viability is expressed as a percentage relative to vehicle controls.

Molecular profiling

PTEN and PIP4K2A were assessed by immunoblot in the patient-derived panel, with GAPDH as loading control. Blot images were acquired and cropped in accordance with journal image-integrity requirements, retaining sufficient flanking bandwidth around the bands of interest; no high-contrast processing was applied. Uncropped, unprocessed scans of all blots are provided as a Supplementary Information file, as required by Scientific Reports.

For immunoblotting, blots were incubated with PIP4K2A 1:1,000 (AP8041b; Abgent), PTEN 1:1,000 (9188S; Cell Signaling), or GAPDH 1:1,000 (SC-47724; Santa Cruz Biotechnology) overnight at 4°C. After washing with Tris-buffered saline with Tween 20, the blots were incubated with HRP-conjugated secondary antibody for 1 h at room temperature. Detection was performed by using the Super Signal West Pico Chemiluminescent Substrate (ECL; Thermo Scientific Pierce).

Murine glioma comparison

GL26 (PTEN-deficient) and GL261 (PTEN-expressing) murine glioma cells were used as biologically distinct PTEN-differential models. They were not treated as a genetically matched pair. Cells were exposed to peptide, randomized-sequence control, or temozolomide (200 μg/mL peptide or 500 μM temozolomide), and viability was measured relative to untreated controls. Their provenance and culture conditions are described above.

Subcutaneous xenograft study

The animal study is reported in accordance with the ARRIVE 2.0 guidelines [34]. All animal procedures were approved by the Institutional Animal Care and Use Committee (IACUC) of Samsung Medical Center

(Approval No. 20230718002) and performed in accordance with the Association for Assessment and Accreditation of Laboratory Animal Care (AAALAC)-accredited guidelines. Female BALB/c nude mice (4–5 weeks of age, approximately 20 g body weight) were housed in a specific pathogen-free (SPF) facility maintained at 22 ± 2°C with 50 ± 10% relative humidity under a 12-hour light/dark cycle, with ad libitum access to sterilized rodent chow and water. To establish subcutaneous xenografts, mice were inoculated with PDC4 cells at twice the total cohort size required for efficacy testing. Five days post-inoculation, mice that developed tumors measuring approximately 50 mm^3 were selectively enrolled, while mice with ulcerated, necrotic, or improperly sized tumors outside this threshold were excluded. Eligible mice were then randomized into four treatment arms (n = 3 per group): vehicle control, PIP4-1, PIP8-1, and PIP4/12 – 1. All peptide test candidates were dissolved in phosphate-buffered saline (PBS) and administered intraperitoneally (IP) at a dose of 100 mg/kg in a standardized volume of 10 ml/kg body weight. Dosing commenced on day 5 post-cell inoculation and continued every two days (Q2D) through day 34, totaling 15 doses per mouse. Tumor size was measured twice weekly using digital calipers by an investigator blinded to treatment allocation.

Tumor volume (V) was calculated as $V = (L \times W^2)/2$, where L is the longest diameter and W is the perpendicular shortest diameter.

Mice were monitored daily for general health status. Predefined humane endpoints included tumor volume exceeding 1,500 mm^3, tumor ulceration, or body weight loss exceeding 20% of baseline; no animal reached these humane termination criteria during the study period. At study completion (day 34), all mice were euthanized by carbon dioxide (CO_2) inhalation: animals were placed in a CO_2 chamber without pre-filling, and chamber air was displaced with 100% compressed CO_2 gas at a slow fill rate of 30% of the chamber volume per minute for 5 min. Decapitation was then performed as a secondary physical method to confirm complete and irreversible death. Euthanasia was carried out in accordance with the AVMA Guidelines for the Euthanasia of Animals (2020 edition) and with institutional IACUC protocol No. 20230718002. The excised tumors were weighed and photographed for downstream analysis

Tolerability assays

HaCaT keratinocytes were exposed to PIP4-1 at 200, 400, and 800 µg/mL. Normal human liver organoids were evaluated across a six-point series (0, 0.781, 3.125, 12.5, 50, and 200 µg/mL) for PIP4-1, PIP8-1, and PIP12-1, and in a separate fixed-dose comparison of PIP4-1, PIP8-1, PIP12-1, PIP4/12 – 1, and temozolomide (Fig. 5). Albumin secretion was measured at days 4 and 7; the calibration curve is shown in Fig. 5F. These assays provide cellular viability and albumin readouts rather than systemic toxicology.

Statistical analysis

Analyses were performed in GraphPad Prism 6.07. Data are presented using the summary measures displayed in the source figures. For inferential in vitro comparisons, one-way analysis of variance with

multiplicity-adjusted post hoc testing was used where the assumptions and replicate structure permitted. For the murine PTEN-differential comparison (Fig. 2C), an ordinary two-way ANOVA ($\alpha = 0.05$) was performed with cell line (GL261/GL26) and treatment as factors (n = 3 per group). The interaction, cell-line, and treatment effects were all significant (interaction: $F(4,20) = 34.40$, $P < 0.0001$; cell line: $F(1,20) = 74.99$, $P < 0.0001$; treatment: $F(4,20) = 59.63$, $P < 0.0001$). Follow-up comparisons within each treatment (GL261 vs GL26) used multiple unpaired t tests with correction for multiple comparisons (two-stage step-up method of Benjamini, Krieger, and Yekutieli); a significant difference between cell lines survived correction only for PIP4-1 ($P = 4.69 \times 10^{-5}$). PIP8-1 had a nominally low uncorrected P value (0.0050) that did not survive correction, and PIP12-1, PIP4/12 − 1, and temozolomide were not significant (P = 0.836, 0.105, and 0.194, respectively). For Fig. 3 (PDC1, panels A–D; PDC4, panels E–H), each peptide was analyzed by a separate ordinary one-way ANOVA with Dunnett's multiple comparisons test against the untreated control (n = 5 per group); each peptide at 40 μg/mL alone versus 40 μg/mL plus temozolomide was additionally compared by an unpaired two-tailed t test, with an F test for equality of variances. For Fig. 2B, each treatment was analyzed by a separate ordinary one-way ANOVA (n = 3 per group; Brown–Forsythe test not significant for any treatment), followed by Dunnett's multiple comparisons test against the untreated control. For the pilot xenograft cohort (n = 3 per group), terminal tumor volumes (Fig. 4C) were compared exploratorily by ordinary one-way ANOVA followed by Dunnett's test against vehicle; this cohort was not powered for formal efficacy testing and the results should be interpreted accordingly. Longitudinal tumor-volume trajectories (Fig. 4A) are described using individual values and group means without formal statistical testing.

[Important: the submitted version stated that "exact n values, definitions of biological and technical replication, error-bar definitions, adjusted P values, and the post hoc procedure remain to be reported" for Figs. 1C, 1D and 5. Scientific Reports requires these for every panel, and an explicit statement that they are missing is likely to prompt an editorial return before review. Please supply them, and delete this note.

Ethics declarations

The use of human-derived tumor and liver materials was approved by the Samsung Medical Center Institutional Review Board (Approval No. 2010-04-004 for tumor and Approval No. 2021-09-112 for liver), and written informed consent was obtained from all participants in accordance with applicable regulations and with the Declaration of Helsinki. All animal procedures were approved by the Institutional Animal Care and Use Committee of Samsung Medical Center (Approval No. 20230718002) and were conducted in accordance with institutional and national guidelines and with the ARRIVE 2.0 guidelines [34].

Abbreviations

GBM
glioblastoma

MGMT
O6-methylguanine-DNA methyltransferase
MTT
3-(4,5-dimethylthiazol-2-yl)-2,5-diphenyltetrazolium bromide
NHA
normal human astrocyte
PDC
patient-derived culture
PI3K
phosphoinositide 3-kinase
PIP4K2A
phosphatidylinositol-5-phosphate 4-kinase type 2 alpha
PTEN
phosphatase and tensin homolog
TMZ
temozolomide.

Declarations

Competing interests

The authors declare no competing interests.

Author Contribution

Conceptualization, Y.-J.K. and Y.J.S.; investigation, Y.O. and J.K.; writing—original draft preparation, Y.-J.K. and Y.J.S.; writing—review and editing, Y.-J.K. and Y.J.S.; supervision, Y.J.S.; funding acquisition, Y.-J.K. and Y.J.S. All authors reviewed and approved the final manuscript

Acknowledgement

This work was supported by the National Research Foundation of Korea (NRF) grant funded by the Korea government (MSIT) (No. RS-2024-00341405), and by the Ministry of Research and Higher Education (MESR) of Luxembourg under the Personalized Functional Profiling (PFP) program and the COLOPAN study.AI-assisted tools were used to support English-language editing and to reorganize and condense manuscript text into the journal’s required format. All scientific content, data, and conclusions are the authors’ own, and the authors reviewed and verified all AI-assisted edits before submission

Data Availability

The datasets generated and analysed during the current study are available in the figshare repository, https://doi.org/10.6084/m9.figshare.34056168. Source data for Figures 1-5, including individual-animal tumor-volume and body-weight measurements and uncropped immunoblot scans, are included in that deposit. No data types requiring mandatory deposition in a community repository (nucleotide or protein sequences, genetic polymorphisms, linked genotype-phenotype data, macromolecular structures, gene expression datasets, or small-molecule crystallographic data) were generated in this study. Additional de-identified data are available from the corresponding author on reasonable request, subject to applicable consent and institutional governance restrictions.

References

1. Jamshidi, P. & Brat, D. J. The 2021 WHO classification of central nervous system tumors: what neurologists need to know. *Curr. Opin. Neurol.* **35**, 764–771. 10.1097/WCO.0000000000001109 (2022).
2. Weller, M. et al. EANO guidelines on the diagnosis and treatment of diffuse gliomas of adulthood. *Nat. Rev. Clin. Oncol.* **18**, 170–186. 10.1038/s41571-020-00447-z (2021).
3. Wen, P. Y. et al. Glioblastoma in adults: A Society for Neuro-Oncology (SNO) and European Society of Neuro-Oncology (EANO) consensus review on current management and future directions. *Neuro Oncol.* **27**, 2751–2788. 10.1093/neuonc/noaf177 (2025).
4. Stupp, R. et al. Effects of radiotherapy with concomitant and adjuvant temozolomide versus radiotherapy alone on survival in glioblastoma in a randomised phase III study: 5-year analysis of the EORTC-NCIC trial. *Lancet Oncol.* **10**, 459–466. 10.1016/S1470-2045(09)70025-7 (2009).
5. Stupp, R. et al. Radiotherapy plus concomitant and adjuvant temozolomide for glioblastoma. *N Engl. J. Med.* **352**, 987–996. 10.1056/NEJMoa043330 (2005).
6. Patel, A. P. et al. Single-cell RNA-seq highlights intratumoral heterogeneity in primary glioblastoma. *Science* **344**, 1396–1401. 10.1126/science.1254257 (2014).
7. Neftel, C. et al. An Integrative Model of Cellular States, Plasticity, and Genetics for Glioblastoma. *Cell* 178, 835–849 e821, (2019). 10.1016/j.cell.2019.06.024
8. Brennan, C. W. et al. The somatic genomic landscape of glioblastoma. *Cell* **155**, 462–477. 10.1016/j.cell.2013.09.034 (2013).
9. Cancer Genome Atlas Research, N. Comprehensive genomic characterization defines human glioblastoma genes and core pathways. *Nature* **455**, 1061–1068. 10.1038/nature07385 (2008).
10. Verhaak, R. G. et al. Integrated genomic analysis identifies clinically relevant subtypes of glioblastoma characterized by abnormalities in PDGFRA, IDH1, EGFR, and NF1. *Cancer Cell.* **17**, 98–110. 10.1016/j.ccr.2009.12.020 (2010).
11. van den Bent, M. J. et al. Updated EANO guideline on rational molecular testing of gliomas, glioneuronal, and neuronal tumors in adults for targeted therapy selection-Update 1. *Neuro Oncol.*

27, 331–337. 10.1093/neuonc/noae213 (2025).

12. Di Cristofano, A. & Pandolfi, P. P. The multiple roles of PTEN in tumor suppression. *Cell* **100**, 387–390. 10.1016/s0092-8674(00)80674-1 (2000).
13. Hopkins, B. D., Hodakoski, C., Barrows, D., Mense, S. M. & Parsons, R. E. PTEN function: the long and the short of it. *Trends Biochem. Sci.* **39**, 183–190. 10.1016/j.tibs.2014.02.006 (2014).
14. Li, J. et al. PTEN, a putative protein tyrosine phosphatase gene mutated in human brain, breast, and prostate cancer. *Science* **275**, 1943–1947. 10.1126/science.275.5308.1943 (1997).
15. Hashemi, M. et al. Progress in targeting PTEN/PI3K/Akt axis in glioblastoma therapy: Revisiting molecular interactions. *Biomed. Pharmacother*. **158**, 114204. 10.1016/j.biopha.2022.114204 (2023).
16. Song, M. S., Salmena, L. & Pandolfi, P. P. The functions and regulation of the PTEN tumour suppressor. *Nat. Rev. Mol. Cell. Biol.* **13**, 283–296. 10.1038/nrm3330 (2012).
17. Chalhoub, N. & Baker, S. J. PTEN and the PI3-kinase pathway in cancer. *Annu. Rev. Pathol.* **4**, 127–150. 10.1146/annurev.pathol.4.110807.092311 (2009).
18. Shin, Y. J. et al. PIP4K2A as a negative regulator of PI3K in PTEN-deficient glioblastoma. *J. Exp. Med.* **216**, 1120–1134. 10.1084/jem.20172170 (2019).
19. Gori, A., Lodigiani, G., Colombarolli, S. G., Bergamaschi, G. & Vitali, A. Cell Penetrating Peptides: Classification, Mechanisms, Methods of Study, and Applications. *ChemMedChem* 18, e202300236, (2023). 10.1002/cmdc.202300236
20. Guidotti, G., Brambilla, L. & Rossi, D. Cell-Penetrating Peptides: From Basic Research to Clinics. *Trends Pharmacol. Sci.* **38**, 406–424. 10.1016/j.tips.2017.01.003 (2017).
21. Sharma, K., Sharma, K. K., Sharma, A. & Jain, R. Peptide-based drug discovery: Current status and recent advances. *Drug Discov Today*. **28**, 103464. 10.1016/j.drudis.2022.103464 (2023).
22. Wang, L. et al. Therapeutic peptides: current applications and future directions. *Signal. Transduct. Target. Ther.* **7** 10.1038/s41392-022-00904-4 (2022).
23. Kauffman, W. B., Fuselier, T., He, J. & Wimley, W. C. Mechanism Matters: A Taxonomy of Cell Penetrating Peptides. *Trends Biochem. Sci.* **40**, 749–764. 10.1016/j.tibs.2015.10.004 (2015).
24. Zhang, H. et al. Recent Advances of Cell-Penetrating Peptides and Their Application as Vectors for Delivery of Peptide and Protein-Based Cargo Molecules. *Pharmaceutics* 15, (2023). 10.3390/pharmaceutics15082093
25. Golebiewska, A. et al. Patient-derived organoids and orthotopic xenografts of primary and recurrent gliomas represent relevant patient avatars for precision oncology. *Acta Neuropathol.* **140**, 919–949. 10.1007/s00401-020-02226-7 (2020).
26. Hubert, C. G. et al. A Three-Dimensional Organoid Culture System Derived from Human Glioblastomas Recapitulates the Hypoxic Gradients and Cancer Stem Cell Heterogeneity of Tumors Found In Vivo. *Cancer Res.* **76**, 2465–2477. 10.1158/0008-5472.CAN-15-2402 (2016).
27. Lanskikh, D. et al. Cell-Based Glioma Models for Anticancer Drug Screening: From Conventional Adherent Cell Cultures to Tumor-Specific Three-Dimensional Constructs. *Cells* 13, (2024).

10.3390/cells13242085

28. Jacob, F. et al. A Patient-Derived Glioblastoma Organoid Model and Biobank Recapitulates Inter- and Intra-tumoral Heterogeneity. *Cell* 180, 188–204 e122, (2020). 10.1016/j.cell.2019.11.036
29. Logun, M. et al. Patient-derived glioblastoma organoids as real-time avatars for assessing responses to clinical CAR-T cell therapy. *Cell Stem Cell* 32, 181–190 e184, (2025). 10.1016/j.stem.2024.11.010
30. Qu, S. et al. Patient-derived organoids in human cancer: a platform for fundamental research and precision medicine. *Mol. Biomed.* **5**, 6. 10.1186/s43556-023-00165-9 (2024).
31. Byrne, A. T. et al. Interrogating open issues in cancer precision medicine with patient-derived xenografts. *Nat. Rev. Cancer*. **17**, 254–268. 10.1038/nrc.2016.140 (2017).
32. Tentler, J. J. et al. Patient-derived tumour xenografts as models for oncology drug development. *Nat. Rev. Clin. Oncol.* **9**, 338–350. 10.1038/nrclinonc.2012.61 (2012).
33. Hidalgo, M. et al. Patient-derived xenograft models: an emerging platform for translational cancer research. *Cancer Discov*. **4**, 998–1013. 10.1158/2159-8290.CD-14-0001 (2014).
34. Percie du Sert. The ARRIVE guidelines 2.0: Updated guidelines for reporting animal research. *PLoS Biol.* **18**, e3000410. 10.1371/journal.pbio.3000410 (2020).

Figures

Figure 1. Design, structural mapping, and initial screening of PIP4K2A-derived peptides

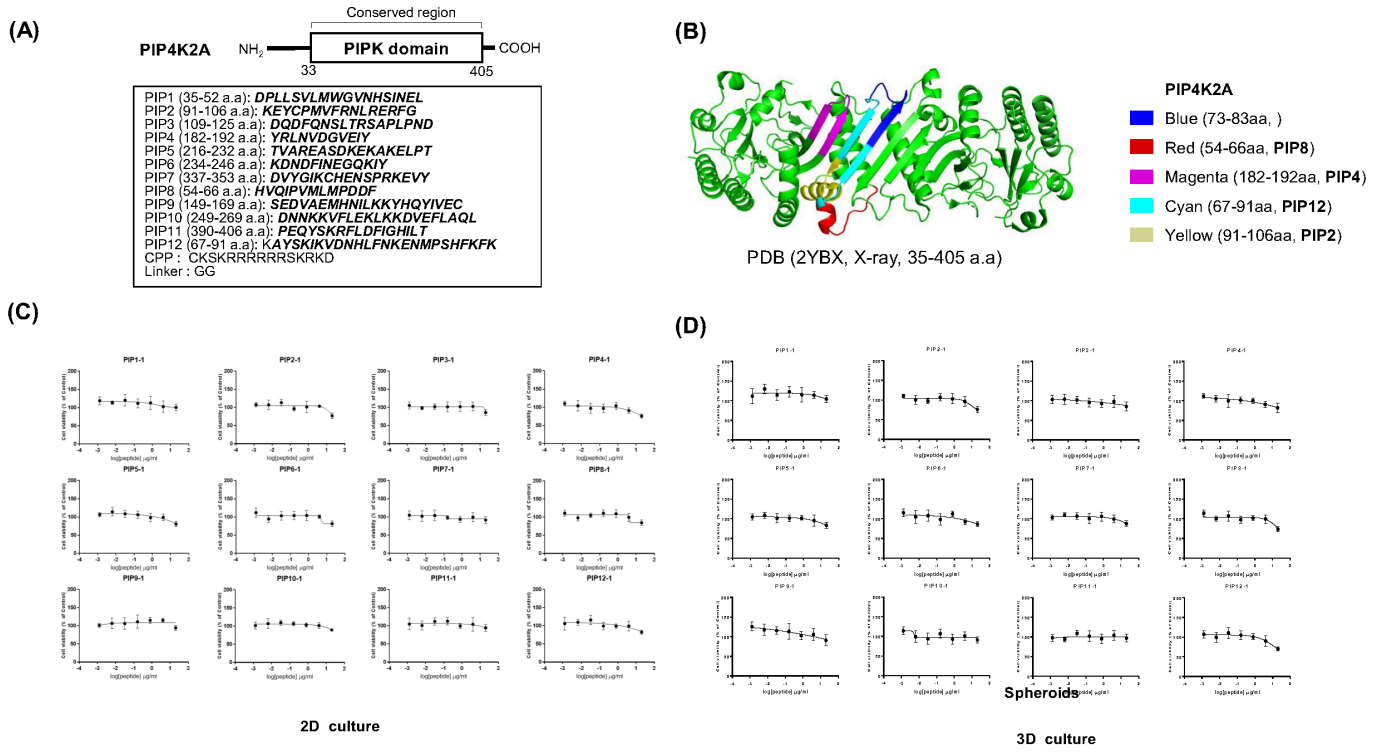


Figure 1

Design, structural mapping, and initial screening of PIP4K2A-derived peptides.

(A) PIP4K2A domain diagram and sequences of 12 candidate regions, together with the GG linker and polybasic carrier. (B) Candidate-region mapping on the PIP4K2A crystal structure (PDB 2YBX, residues 35–405). Highlighted regions include PIP8 (residues 54–66), PIP12 (67–91), PIP2 (91–106), PIP4 (182–192), and a segment at residues 73–83. The mapping identifies sequence origin and does not demonstrate functional mimicry. (C) Concentration-response screening in PDC1 dissociated 2D cultures. (D) Corresponding screening in PDC1 3D spheroids. Viability is expressed as a percentage of control. For panels C and D, each condition was assayed in 3–5 replicate wells per experiment across at least three independent biological experiments; n therefore denotes independent biological replicates (n ≥ 3). Symbols show the mean and error bars indicate s.d.

Figure 2. Molecular characterization and activity of selected PIP4K2A-derived peptides

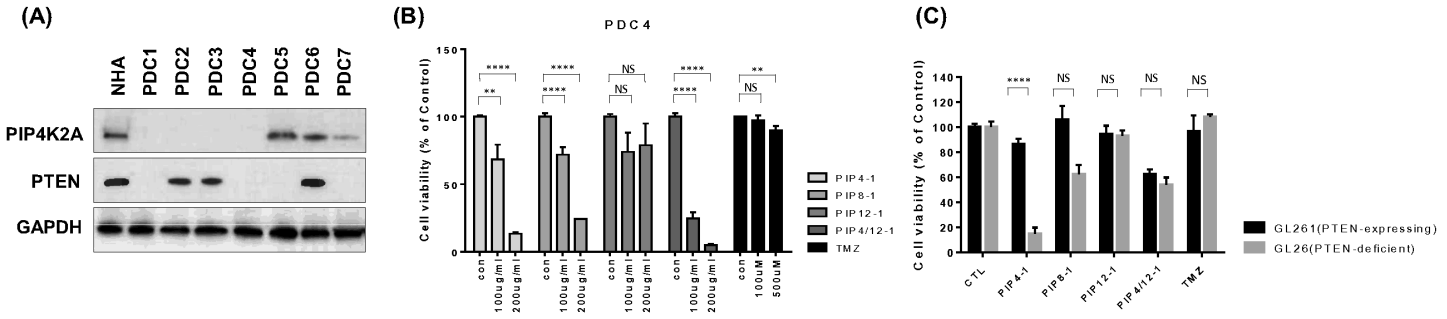


Figure 2

Molecular characterization and activity of selected PIP4K2A-derived peptides.

(A) PIP4K2A and PTEN immunoblots in NHA and PDC1–PDC7, with GAPDH as loading control; uncropped scans are provided in Supplementary Figure S5. (B) Fixed-dose viability responses to PIP4-1, PIP8-1, PIP12-1, PIP4/12-1, and temozolomide in PDC4 (ordinary one-way ANOVA per treatment; significant overall effect for PIP4-1: $F(2,6) = 140.8$, $P < 0.0001$, $R^2 = 0.9791$; PIP8-1: $F(2,6) = 350.4$, $P < 0.0001$, $R^2 = 0.9915$; PIP4/12-1: $F(2,6) = 774.4$, $P < 0.0001$, $R^2 = 0.9961$; not significant for PIP12-1: $F(2,6) = 3.677$, $P = 0.0907$, $R^2 = 0.5507$; temozolomide reached overall significance, $F(2,6) = 9.713$, $P = 0.0131$, $R^2 = 0.7640$, but with a much smaller effect size and a maximal reduction of only ~10%; Dunnett's test vs

control: PIP4-1 100/200 µg/mL P < 0.01 / P < 0.0001; PIP8-1 100/200 µg/mL P < 0.001 / P < 0.0001; PIP12-1 100/200 µg/mL ns/ns; PIP4/12-1 100/200 µg/mL P < 0.0001 / P < 0.0001; temozolomide 100/500 µM ns / P < 0.01). (C) Exploratory comparison of peptide and temozolomide responses in PTEN-expressing GL261 and PTEN-deficient GL26 cells (two-way ANOVA; interaction, cell-line, and treatment effects all P < 0.0001; n = 3 per group). Follow-up comparisons within each treatment (GL261 vs GL26) used multiple unpaired t tests with correction for multiple comparisons (two-stage step-up method of Benjamini, Krieger, and Yekutieli); a significant difference survived correction only for PIP4-1 ($P = 4.69 \times 10^{-5}$, ****). PIP8-1 had a nominally low uncorrected P value (0.0050) that did not survive correction; PIP12-1, PIP4/12-1, and temozolomide were not significant (P = 0.836, 0.105, and 0.194, respectively). PDC7 showed weakly detected PIP4K2A and no detectable PTEN on the same immunoblot (panel A). Each condition was assayed in 3–5 replicate wells per experiment across at least three independent biological experiments; n therefore denotes independent biological replicates (n ≥ 3). Symbols show the mean and error bars indicate s.d.

Figure 3. Fixed-dose responses to PIP4K2A-derived peptides and temozolomide in patient-derived cultures

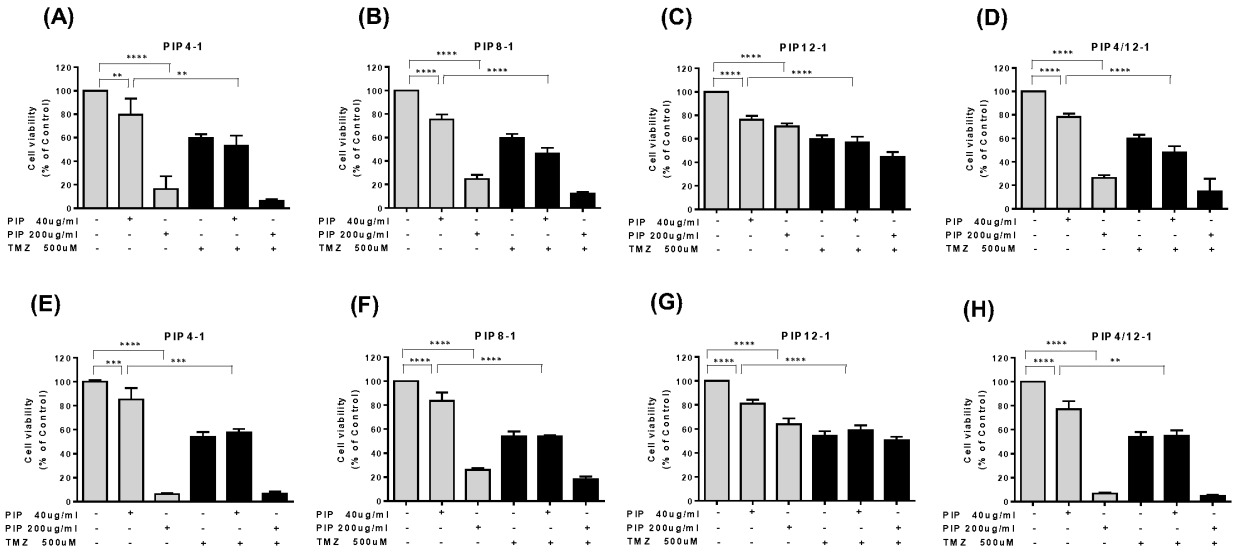


Figure 3

Fixed-dose responses to PIP4K2A-derived peptides and temozolomide in patient-derived cultures.

Viability of PDC1 and PDC4 after PIP4-1, PIP8-1, PIP12-1, or PIP4/12-1 at 40 or 200 µg/mL, temozolomide at 500 µM, or the indicated combinations. PIP4-1 at 200 µg/mL produced a greater viability reduction than temozolomide alone in both models. Dunnett's multiple comparisons test showed that every dose, temozolomide, and combination condition differed significantly from control in

both models (PDC1, panels A–D: P < 0.01 for PIP4-1 at 40 µg/mL, P < 0.0001 for all other conditions; PDC4, panels E–H: P < 0.001 for PIP4-1 at 40 µg/mL, P < 0.0001 for all other conditions). Unpaired t tests showed that 40 µg/mL plus temozolomide produced a significantly greater reduction than 40 µg/mL peptide alone for every peptide in both models (PDC1: P = 0.0067 to P < 0.0001; PDC4: P = 0.0003 to P < 0.0001). F tests indicated significantly unequal variances for PIP4-1 and PIP8-1 in PDC4 (P = 0.038 and P = 0.0066); these two comparisons were therefore repeated with Welch's correction, which did not change their significance. Each condition was assayed in 5 replicate wells per experiment across at least three independent biological experiments; n therefore denotes independent biological replicates (n ≥ 3). Symbols show the mean and error bars indicate s.d.

Figure 4. Pilot antitumor activity in a subcutaneous xenograft model

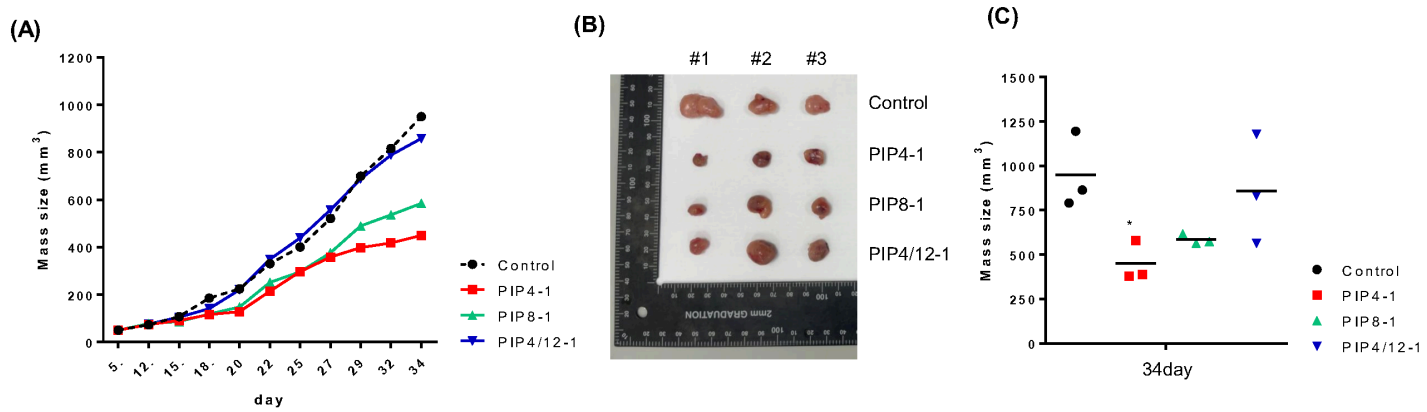


Figure 4

Pilot antitumor activity in a subcutaneous PDX4 xenograft model.

Longitudinal mean tumor volume, representative excised tumors, and individual terminal tumor volumes are shown for vehicle, PIP4-1, PIP8-1, and PIP4/12-1 (100 mg/kg; n = 3 per group). The x-axis displays study days 5–34, corresponding to 29 days of longitudinal observation. Terminal tumor volumes differed overall by one-way ANOVA ($F(3,8) = 4.227$, $P = 0.0458$, $R^2 = 0.6132$); Dunnett's test showed a significant reduction for PIP4-1 versus vehicle (mean difference 500.9 mm^3, 95% CI 38.9–962.9, $P < 0.05$) but not for PIP8-1 (mean difference 365.6 mm^3, 95% CI −96.4 to 827.6, ns) or PIP4/12-1 (mean difference 92.5 mm^3, 95% CI −369.5 to 554.5, ns). The cohort was not powered for formal efficacy testing.

Figure 5. Preliminary tolerability in nonmalignant models

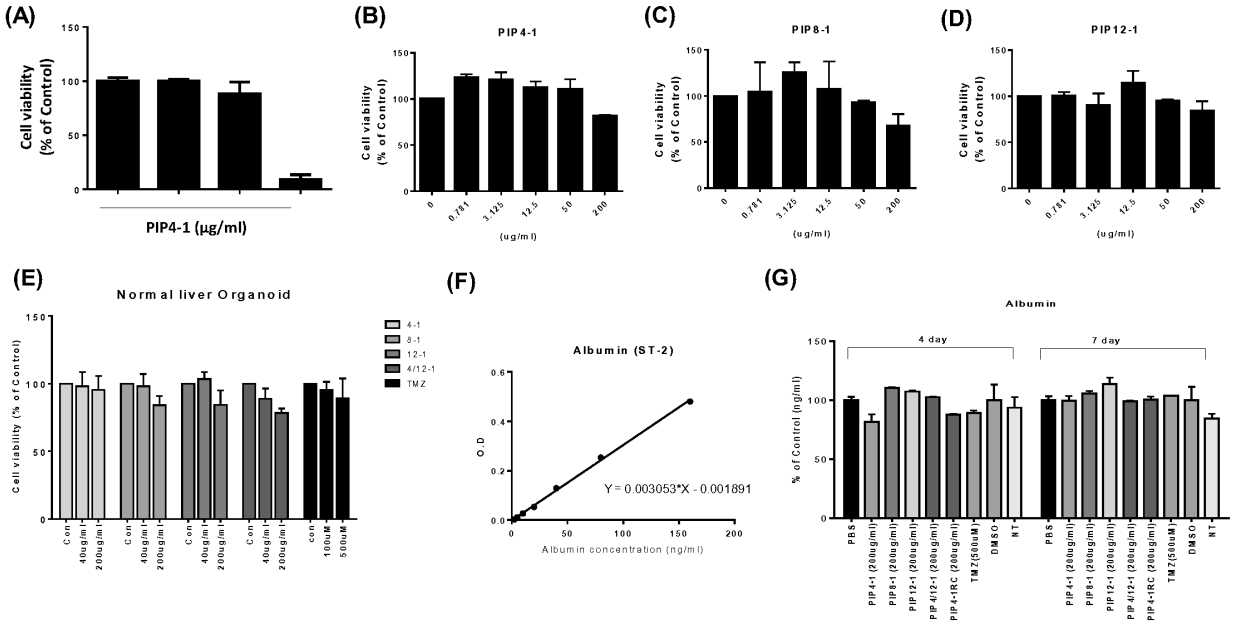


Figure 5

Preliminary tolerability in nonmalignant models.

(A) HaCaT keratinocyte viability after PIP4-1 at 200, 400, and 800 μg/mL. (B–D) Normal human liver-organoid viability after PIP4-1, PIP8-1, or PIP12-1 across 0–200 μg/mL. (E) Separate liver-organoid viability comparison after PIP4-1, PIP8-1, PIP12-1, PIP4/12-1, or temozolomide at the indicated concentrations. (F) Albumin calibration curve. (G) Albumin measurements at days 4 and 7 after peptide, temozolomide, or control treatment. These experiments evaluate acute cellular responses and do not constitute systemic toxicology. Each condition was assayed in 3 replicate wells per experiment across at least three independent biological experiments; n therefore denotes independent biological replicates ($n \geq 3$). Symbols show the mean and error bars indicate s.d.

Supplementary Files

This is a list of supplementary files associated with this preprint. Click to download.

- SupplementaryTableS1S220260928.pdf
- SupplementaryTableS1S220260929.docx
- SupplementaryInformation.docx